Environmental Sciences Europe

RESEARCH

Open Access

Carbonaceous composite materials from calcination of azo dye-adsorbed layered double hydroxide with enhanced photocatalytic efficiency for removal of Ibuprofen in water

Xiaolin Shen[1,2], Zhiliang Zhu[1,2,3*], Hua Zhang[2,3], Guanglan Di[1,2], Ting Chen[1,2], Yanling Qiu[1,3] and Daqiang Yin[1,3]

Abstract

Background: The discard of used adsorbents may pose a great threat to human health and ecological environment. This work herein reported a facile and feasible method, with aims of (i) reusing the calcined layered double hydroxide (CLDH) adsorbent after azo dye adsorption, and (ii) being further used as a photocatalyst to enhance the degradation of typical pharmaceuticals. Calcination under inner gas flow has been utilized to carbonize adsorbed azo dye and a kind of novel carbonaceous CLDH composite material (CM-CLDH) was synthesized. This fabricated material was used as a catalyst for Ibuprofen removal in water samples under simulated sunlight irradiation.

Results: According to our experimental results, combination of carbonaceous material with CLDH showed an enhanced photocatalytic performance compared to original CLDH materials. More than 90% of Ibuprofen could be removed in less than 180 min. Introduction of carbon material narrowed catalyst's band gap and turned its conduct band potential to a more negative state, which brought considerable light absorption and higher oxidation ability of photo-induced electrons. Furthermore, photoluminescent spectra and transient photocurrent examination confirmed that carbon material suppressed recombination of photo-induced electrons and holes through faster electron transportation. Under experimental conditions, the removal efficiency of Ibuprofen by CM-CLDH composite kept above 90% during five cycles.

Conclusion: Calcination under inner gas flow can transform organic pollutant-adsorbed CLDH to CM-CLDH composite with higher photocatalytic performance. A feasible way to reuse spent LDH adsorbents was proposed, which is a benefit to reduce second pollution of spent adsorbents in environment.

Keywords: Layered double hydroxide, Carbonaceous material, Photodegradation, Ibuprofen, Spent adsorbent reuse

Background

Azo dyes draw enormous attention for causing mutation and carcinoma through aromatic amines [1], and they are likely to trigger foul smell, eutrophication, and decrease of dissolved oxygen amount when released into natural water, posing a threat to humans and aquatic ecosystem [2, 3]. Adsorption [4], electrocatalysis [5] and photocatalysis [6] have been applied to deal with azo dye wastewater; among them, adsorption is preferred for its low cost, simple operation, high removal efficiency and reusability [7, 8].

Layered double hydroxide (LDH) is a kind of hydrotalcite-like compounds, denoted as $[M^{2+}_{(1-x)}M^{3+}_{x}(OH)_2]_{layer}[A^{n-}_{x/n}\cdot zH_2O]_{interlayer}$, where M^{2+}, M^{3+} and A^{n-} represent divalent, trivalent metal cations

*Correspondence: zzl@tongji.edu.cn
[1] Key Laboratory of Yangtze River Water Environment, Ministry of Education, Tongji University, Shanghai 200092, China
Full list of author information is available at the end of the article

and interlayer anions, respectively [4]. LDHs have been regarded as a kind of effective adsorbents attributing to their tunable charge densities and large specific surface areas [8], the interlayer anions can exchange with anions from contaminants [9], and large specific surface areas can provide with sufficient adsorption sites and reactive hydroxy for ligand exchange [10]. When calcined at moderate temperatures (400–500 °C), LDH's layered structure will collapse owing to interlayer anions' decomposition and release of interlayer water. Normally, calcined LDH (CLDH) exhibits favorable adsorption capacity and efficiency due to larger specific surface areas and lamellar structure's reconstruction, and researchers regard it as a kind of promising adsorbent for azo dye treatment [11, 12].

After adsorption of anions from wastewater, treatment of spent LDHs becomes a tough challenge. Normal landfilling or piling up may result in foul smell, contamination of soil and underground water by leachate [13]. According to limited research consequences, after adsorption, Laipan et al. [13] fabricated carbon-LDH composites via calcination under inert gas flow. The resulting material was efficient for Cr(VI) reduction, and it would be converted to metal ions and porous carbon through pickling. Metal ions were utilized for LDH synthesis once again, and porous structure was promising for toluene adsorption [14]. Nevertheless, researches related to using combination of organic pollutant-based carbonaceous material and LDH for photocatalysis are still limited. As mentioned in former research articles, addition of carbon-based materials like fullerene, graphene oxide (GO) and reduced graphene oxide (rGO) could promote LDH's photocatalytic efficiency. Further study pointed out that combination of LDHs and carbon-based materials would hamper recombination of photo-induced charges and aggregation of LDH layered structures [15, 16]. Ju et al. [17] fabricated fullerene/ZnAlTi-LDO composites; unique electronic properties allowed fullerene to act as an ideal electron acceptor to maintain effective separation of photo-induced electrons and holes. GO and rGO own long-range π–π conjugations, remarkable electron mobility and specific surface area [16, 18, 19]. Zhu et al. pointed out that the electron mediator rGO in rGO/ZnFe-CLDH composite was enabled to improve the migration of electron from conduct band of ZnO to value band of $ZnFe_2O_4$, and Ni et al. argued that high work function of rGO caused movement of electron from value band of LDH to the surface of rGO [19], the aforementioned behavior succeeded in suppressing the recombination of photogenerated charge carriers and leading to an improved photocatalytic efficiency [18]. Apart from graphene-like materials, Mohamed et al. found that union of LDHs and polymer could also boost photocatalytic performance [20], and polypyrrole (Ppy) nanofiber was able to provide larger specific surface area and decrease band gap of pristine LDH, which suggested lower energy consumption during producing single electron or hole, together with light-adsorption of wider wavelength range [21, 22]. As a member of conjugated organic polymer, Ppy's conjugated P-electronic structure led to fast separation efficiency of photo-generated charge carrier, and more electrons and holes could move to the surface then reacted to generate radicals. Researchers also found that carbon materials could have large specific surface area, which was suitable for adsorption [23]. Dong et al. [24] combined agar with normal semiconductor C_3N_4, which made more pollutants adsorbed on the surface of catalyst, and photodegradation efficiency was promoted. Though these mentioned materials facilitate certain photocatalytic performance, high price and relatively complex preparation process still restrict their applications.

To overcome the above deficiencies and make use of advantages of LDH materials, fabricating carbonaceous material and LDH composites (CM-CLDH) derived from spent LDH may reduce the cost of functional materials, avoid secondly environmental pollution from the abandoned adsorbents, and achieve recycling utilization of materials. Therefore, in this work, we focused on preparing carbonaceous functional composite material-CLDH (CM-CLDH) from azo dye-adsorbed CLDH materials through calcination under inert gas protection. Typical azo food colorant amaranth (AM) was selected as dye pollutant and carbon source, and calcined CLDH was chosen as adsorbent. First, adsorption was conducted by CLDH in amaranth solution. Second, spent CLDH was calcined under different temperatures under nitrogen protection to obtain a series of CM-CLDHs. Third, the synthesized CM-CLDHs material was used as a photocatalyst to study the removal performance of the Ibuprofen (IBF), one of the mass-produced and widedistributed acesodyne [25] in water environment. The possible mechanisms of Ibuprofen removal were investigated and discussed. The stability and reusability of the composite CM-CLDHs as photocatalyst were also evaluated. This work can provide a feasible way to synthesize carbonaceous functional material by reusing spent LDH adsorbents, which is also a benefit to reduce second pollution of spent adsorbents in environment.

Materials and methods

Materials

All chemicals were purchased from chemical companies; no purification was operated on them during the experimental process. Zinc nitrate hexahydrate ($Zn(NO_3)_2{\cdot}6H_2O$, AR grade), aluminum nitrate nonahydrate ($Al(NO_3)_3{\cdot}9H_2O$, AR grade), sodium hydroxide

(NaOH, AR grade), sodium carbonate (Na_2CO_3, AR grade), amaranth ($C_{20}H_{11}N_2Na_3O_{10}S_3$, FMP grade) and Ibuprofen ($C_{13}H\text{-}_{18}O_2$, > 98%) were obtained from Sinopharm Chemical Reagent Co., Ltd (China). Lanthanum nitrate hexahydrate ($La(NO_3)_3{\cdot}6H_2O$, AR grade) was purchased from Aladdin Co., Ltd (China). Ultrapure water was produced by a milli-Q device (18.2 MΩ cm at 25 °C).

Preparation of catalysts

Preparation of ZnAlLa-LDH

ZnAlLa-LDH was synthesized via co-precipitation method, 20 mmol $Zn(NO_3)_2{\cdot}6H_2O$, 7.5 mmol $Al(NO_3)_3{\cdot}9H_2O$ and 2.5 mmol $La(NO_3)_3{\cdot}6H_2O$ were put into 50 mL ultrapure water to form stable solution through moderate stir. The mixture of metal nitrates was moved to a burette, then was dropwise added into a 300-mL beaker with 100 mL Na_2CO_3 solution (0.2 mol L^{-1}), and 1 mol L^{-1} NaOH was injected into the beaker via a peristaltic pump to keep solution's pH at 10 ± 0.1. The resulting slurry was stirred on magnetic stirrer for 1 h before sent to drying oven for 24 h' aging. The obtained mixture was filtered by 0.45-μm filter membranes and washed by ultrapure water for three times. In the end, ZnAlLa-LDH was obtained after being dried at 80 °C overnight then ground into powder in mortar.

Preparation of ZnAlLa-CLDH

Aforementioned ZnAlLa-LDH was put in 20-mL crucible before sent to muffle furnace for calcination. Heating rate and heating time were controlled at 10 °C min^{-1} and 240 min. A series of CLDHs were synthesized with heating temperature controlled at 400, 500, and 600 °C, respectively. To distinguish, the obtained materials were successively noted as ZnAlLa-400CLDH, ZnAlLa-500CLDH, and ZnAlLa-600CLDH.

Preparation of CM-CLDH catalyst

According to the screening result of adsorption performance, ZnAlLa-400CLDH presented highest adsorption efficiency among all the prepared ZnAlLa-CLDH materials. As for CM-CLDH fabrication, ZnAlLa-400CLDH was added in 10, 20, 50, and 100 mg/L amaranth with the dosage of 500 mg L^{-1} to establish adsorption equilibrium. To be specific, in dye solution with concentration ranged from 10 to 100 mg/L, amaranth could be thoroughly adsorbed and removed by ZnAlLa-400CLDH. After suction filtration and washed by ultrapure water, the resulting precursor was sent to tube furnace for calcination at 400, 500, and 600 °C under the protection of nitrogen (flow rate = 0.2 L min^{-1}), respectively. Meanwhile, the heating rate and heating time were controlled at 5 °C min^{-1} and 180 min. The final resulting product is named as CM-CLDH, which is a carbonaceous composite CLDH material.

Methods

Characterization

Detection of materials' Crystal phases was performed by a D-8 Advance X-ray diffractometer (Bruker-AXS, Germany) with Cu Ka radiation operated at 40 kV and 40 mA. Fourier transfer infrared (FTIR) spectra were obtained from Thermo Nicolet 5700 (Thermo Nicolet Corporation, USA). Microstructural characterization was carried out via scanning electron microscope (Nova nano SEM 450, FEI, Netherlands) and transmission electron microscope (JEM-2011, JEOL, Japan) equipped with energy-dispersive X-ray spectroscopy (EDX) mapping. X-ray photoelectron spectroscopy (XPS) plot was obtained from Thermo ESCALAB 250XI. Electron spin resonance (ESR) signals were investigated by ESR studio (Freiberg instruments Miniscope MS5000, Germany). Electrochemical properties were measured on electrochemical workstation (biological VSP-300, France).

Adsorption experiments

Batch adsorption experiments were carried out on magnetic stirring apparatus with reaction temperature controlled at 25 ± 5 °C, 100 mL amaranth solution (concentration = 50 mg/L) was poured into 150-mL conical flask, sealed by aluminum foil. A certain amount of LDH/CLDHs (500 mg/L) were added into solution, then solution was stirred at 500 rpm for 6 h. Syringe was used to collect sample at 20, 40, 60, 120, 180, 240, 300, and 360 min after the start of adsorption experiments; the sample solution was filtered by 0.45-μm aqueous phase membrane before examined by UV–vis spectrophotometer (SOPTOP UV2400, China) at wavelength of 520 nm.

Experimental data were fitted by pseudo-first-order and pseudo-second-order kinetic models, two kinds of formulas were listed as follows:

$$\ln(q_e - q_t) = \ln q_e - k_1 t \tag{1}$$

$$\frac{t}{q_t} = \frac{1}{K_2 q_e^2} + \frac{t}{q_e} \tag{2}$$

where q_e and q_t successively represented adsorption capacity of the adsorbent at equilibrium and time t; K_1 (min^{-1}) and K_2 [g (mg min)$^{-1}$] represented adsorption rate constants of these two kinetic models.

In the meantime, adsorption isotherms were determined via batch equilibration method, with temperature set at 25 ± 5 °C. 100 mL dye solution was added into each beaker, concentration of amaranth ranged from 10 to 1000 mg/L, and dosage of adsorbents was 500 mg/L.

After stirred on magnetic stirrer at 500 rpm for 16 h, 2.5 mL of resulting solution was collected by syringe equipped with 0.45-μm aqueous phase membrane in sequence, then examined by UV–vis spectrophotometer at wavelength of 520 nm. Langmuir and Freundlich equation were chosen to assess adsorption behavior of amaranth onto ZnAlLa-400CLDH; the formulas are listed as follows:

$$\frac{C_e}{q_e} = \frac{C_e}{q_{max}} + \frac{1}{K_L q_{max}} \quad (3)$$

$$\log q_e = \log K_F + \frac{1}{n} \log C_e \quad (4)$$

where q_e (mg/g) is equilibrium adsorption capacity of amaranth onto ZnAlLa-400CLDH, q_{max} (mg/g) is the theoretical maximum monolayer sorption capacity, C_e (mg/L) is concentration of dye solution at equilibrium, K_L and K_F are Langmuir and Freundlich adsorption constants.

Photocatalytic experiments

Photodegradation rate of IBF under simulated solar irradiation was applied to assess photocatalytic performance of prepared CM-CLDH composite materials. Simulated solar irradiation was generated by a 500-W xenon lamp (NBeT, China), and light source wavelength was controlled by a 300-nm cut-off filter. Certain amount of IBF solution and catalysts were added into 100-mL quartz tube, mixed with magnetic stir bar. The quartz tubes were immobilized in a ring-like holder with 8 cm distance away from lamp, and the holder could rotate at a constant rate.

The mixture of IBF and catalyst CM-CLDH was magnetically stirred at dark for 30 min to minimize effect of adsorption, followed by light illumination for several hours. About 1 mL reaction solution samples were collected by syringe periodically, and filtered by 0.22-μm water phase membrane to separate solid particles. The concentration of IBF in resulting solution was investigated by ultra-performance liquid chromatography equipped with photodiode array detector (Waters Acquity, USA).

Results and discussions

Characterization

XRD analysis

Figure 1A displays XRD patterns of prepared samples, including original ZnAlLa-LDH, ZnAlLa-CLDH, CLDH-AM and CM-CLDH (CLDH-AM was ZnAlLa-CLDH after adsorption in amaranth solution). As depicted in pattern, spiculate and symmetric peaks at 11.5°, 23.1° and 34.4° which were assigned to (003), (006) and (009) planes indicated prepared materials' lamellar structure [26]. These aforementioned peaks, together with (105), (108), (110) and (113) planes' peaks located at 38.9°, 44.6°, 59.9° and 61.2° illustrated typical crystalline structure of LDH [27]. After calcination, these typical peaks disappeared, manifesting collapse of the original lamellar crystalline structure. With the increase of calcination temperature, peaks of obtained products became sharper, which may attribute to the formation of metal oxide [28]. After adsorption in amaranth solution, CLDH represented characteristic peaks of LDH again, which meant rehydration lamellar hydrotalcite-like structure reconstruction had been accomplished. Referred to former research, the main reason was LDH's intrinsic "memory effect" [29].

FTIR

As shown in Fig. 1B, peaks at around 3450 cm^{-1} were belonged to O–H stretching vibration of water on surface and intercalated into layered double hydroxide [30]. Intensity was weaker in calcined LDH, caused by water loss via calcination. The absorption band stood at 1367 cm^{-1} was connected with asymmetric stretching of interlayer carbonate [31]. Bands located at 500–1000 cm^{-1} region were related to metal–oxygen and metal–hydroxyl vibrations [32]. Asymmetric stretching vibration of S–O was observed at around 1200 cm^{-1} [33], and vibrations at region of 1100–1300 cm^{-1} of CLDH-AM were corresponding to SO_3^{2-} vibrations [31], manifesting amaranth was adsorbed by CLDH.

XPS

Figure 1C, D expounds sectional high-solution XPS spectra of CM-CLDH and used CM-CLDH (catalyst after photocatalysis). Full XPS spectra and high-solution XPS spectra of residual elements are delivered in Additional file 1: Fig. S1. Signals of Zn 2p, Al 2p, La 3d, C 1 s and O 1 s could be detected in both samples. Zn 2p had two peaks at 1021.4 and 1044.6 eV, indicating Zn $2p_{1/2}$ and Zn $2p_{3/2}$ of Zn^{2+}, which could be assigned ZnO and $ZnAl_2O_4$ [28]. Al 2p peak at 74.1 eV proved the existence of Al^{3+} [34].

Original La^{3+} peak was at 834.4 eV [35]. O 1 s peak at 530.9 eV was assigned to metal–oxide chemical bonds [18]. C 1 s peaks at 285.0 and 289.0 eV were attributed to C–C and C=O species [18, 36], indicating that adsorbed amaranth has been transformed into the carbon-based material, which could also be proved by elemental mapping images. After photocatalytic process, binding energy peaks had positive shifts, the probable cause was interaction between Ibuprofen anions and CM-CLDH during reaction, and increase of electronegativity promoted

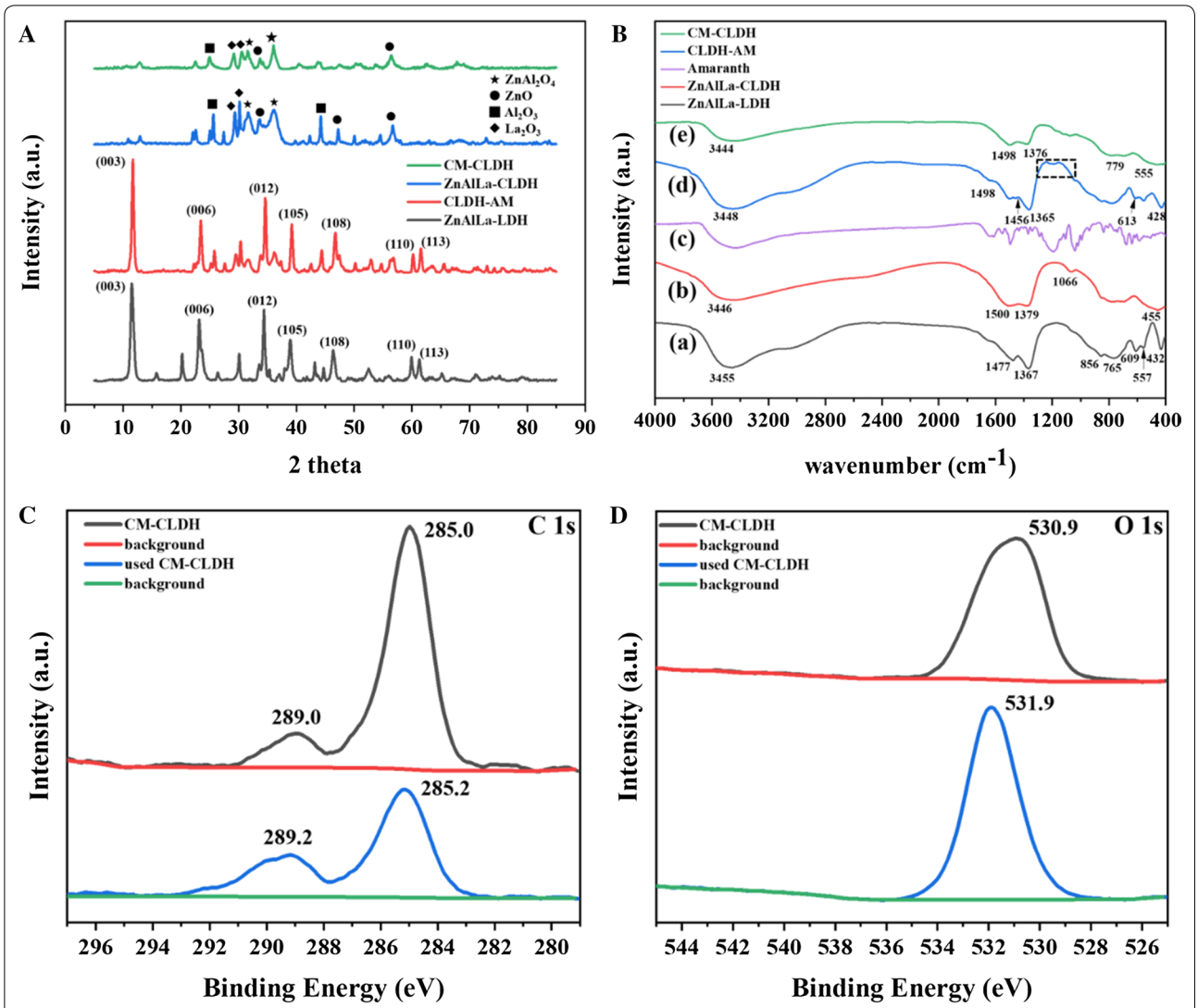

Fig. 1 XRD patterns of prepared materials (**A**), FT-IR spectra of ZnAlLa-LDH (a), ZnAlLa-CLDH (b), amaranth (c), CLDH-AM (d), CM-CLDH (e) (**B**), XPS spectra of C 1 s (**C**) and O 1 s (**D**)

attraction between extranuclear electrons and nuclear, which led to augment of binding energy [35].

Morphology

Figure 2a, b demonstrates exterior structure of synthesized materials. ZnAlLa-CLDH got a sphere-like morphology, stacked by a large number of platelet-like units, which was in accordance with relevant research results [37]. After reaction in amaranth solution, the size of single nanoflakes became larger. Furthermore, a part of nanoflakes exhibited rougher edges; together with some little particles appeared on their surface, these phenomena were caused by adsorption of amaranth.

As displayed in Fig. 2c, d, TEM patterns of CM-CLDH certified this material had a multi-layered structure. Moreover, interplanar spacing was measured by Digital Micrograph software, and three obvious interplanar distances were severally 0.251, 0.193 and 0.243 nm, corresponding to (101), (102) planes of ZnO, and that of (311) planes attributing to $ZnAl_2O_4$. The selected area electron diffraction (SAED) pattern demonstrated through calcination, polycrystalline phase had been constructed in CM-CLDH [38], which could also be proved by XRD patterns.

Elemental mapping analysis had been conducted simultaneously, the results of Fig. 3 elucidated that zinc, aluminum, lanthanum, oxide and carbon were the main

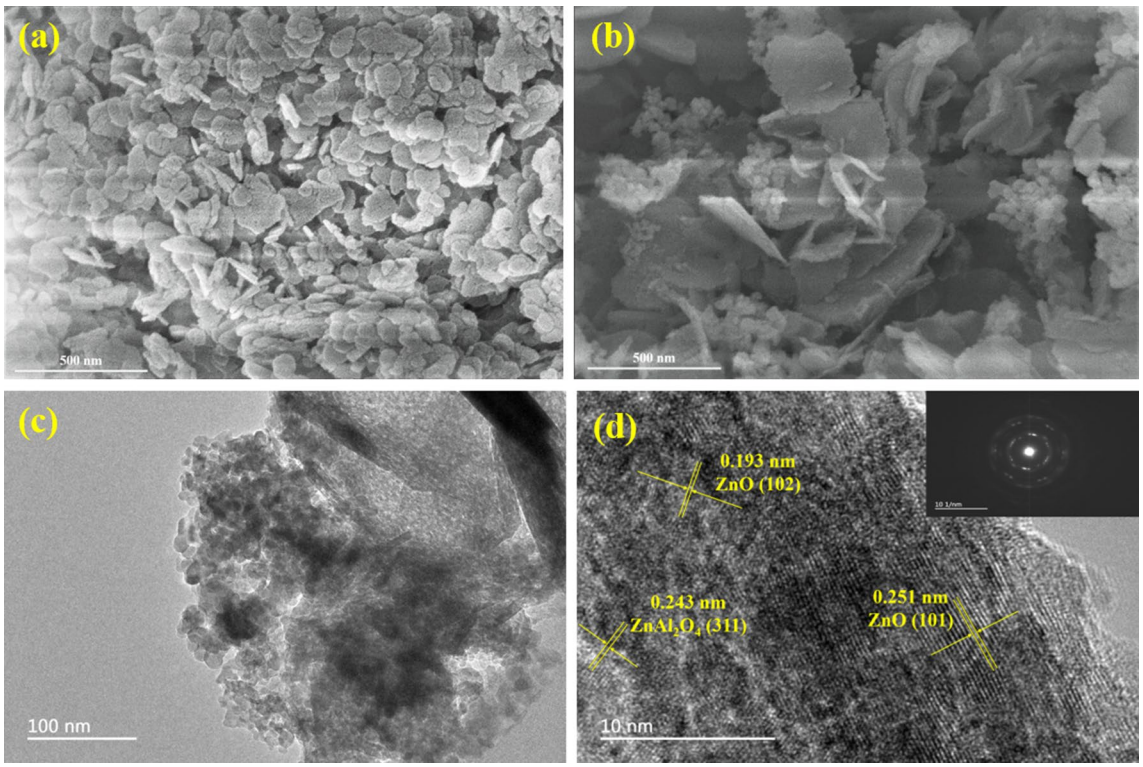

Fig. 2 SEM images of ZnAlLa-CLDH (**a**), CM-CLDH (**b**), TEM image of CM-CLDH (**c**), and HRTEM image and SAED pattern of CM-CLDH (**d**)

components of CM-CLDH. These five elements uniformly dispersed throughout sample, only a part of zinc and lanthanum accompanied with oxygen-constructed sphere-like structure, which might relate to the formation of ZnO and La_2O_3.

Thermal analysis

Additional file 1: Fig. S2 exhibits thermogravimetry curves of synthesized materials and amaranth. As for LDH, weight loss from 50 °C to 168 °C and 168 °C to 242 °C was related to evaporation of water absorbed on the crystalline surface and intercalated into layers successively [4]. The weight of water evaporated accounted for 17.6% of the total weight of LDH. During 242 °C to 336 °C, dehydroxylation and decomposition of some interlaminar carbonate led to 3.7% weight loss. With continuous temperature rise from 336 to 800 °C, residual carbonate decomposed and the lamellar structure collapsed [39].

Amaranth kept stable during 50 °C to 300 °C, and then a rapid weight loss could be spotted with temperature risen from 300 to 800 °C. A great number of aromatic groups might provide amaranth with a prominent thermal stability. When temperature rose to a relevant high range, the aromatic structure triggered carbonation process, which could explain sharp decrease of weight loss [40]. The carbonaceous products remained stable, so there was still 51.9% residue of amaranth left at 800 °C.

Compared with pristine LDH, CLDH-AM suffered from less weight loss in the first step, indicating weaker interaction between LDH and water. In the end, total mass loss of the composite CLDH-AM material was 21.3%, much less than LDH (33.05%), demonstrating the intercalation of amaranth could improve thermal stability and hydrophobicity of LDH [14].

Amaranth adsorption experiments

As shown in Fig. 4a, CLDHs calcined at 400, 500, and 600 °C showed obviously higher adsorption capacity of amaranth than LDH, driven by larger specific surface area and "memory effect" as mentioned previously.

No significant difference had been found on CLDHs' adsorption capacity and rate; calcination temperature had a negligible effect on amaranth adsorption in this experiment. All three adsorbents could reach adsorption equilibrium at 180 min, and ZnAlLa-400CLDH got a relevant higher reaction rate, so this material was chosen for follow-up experiments and characterizations.

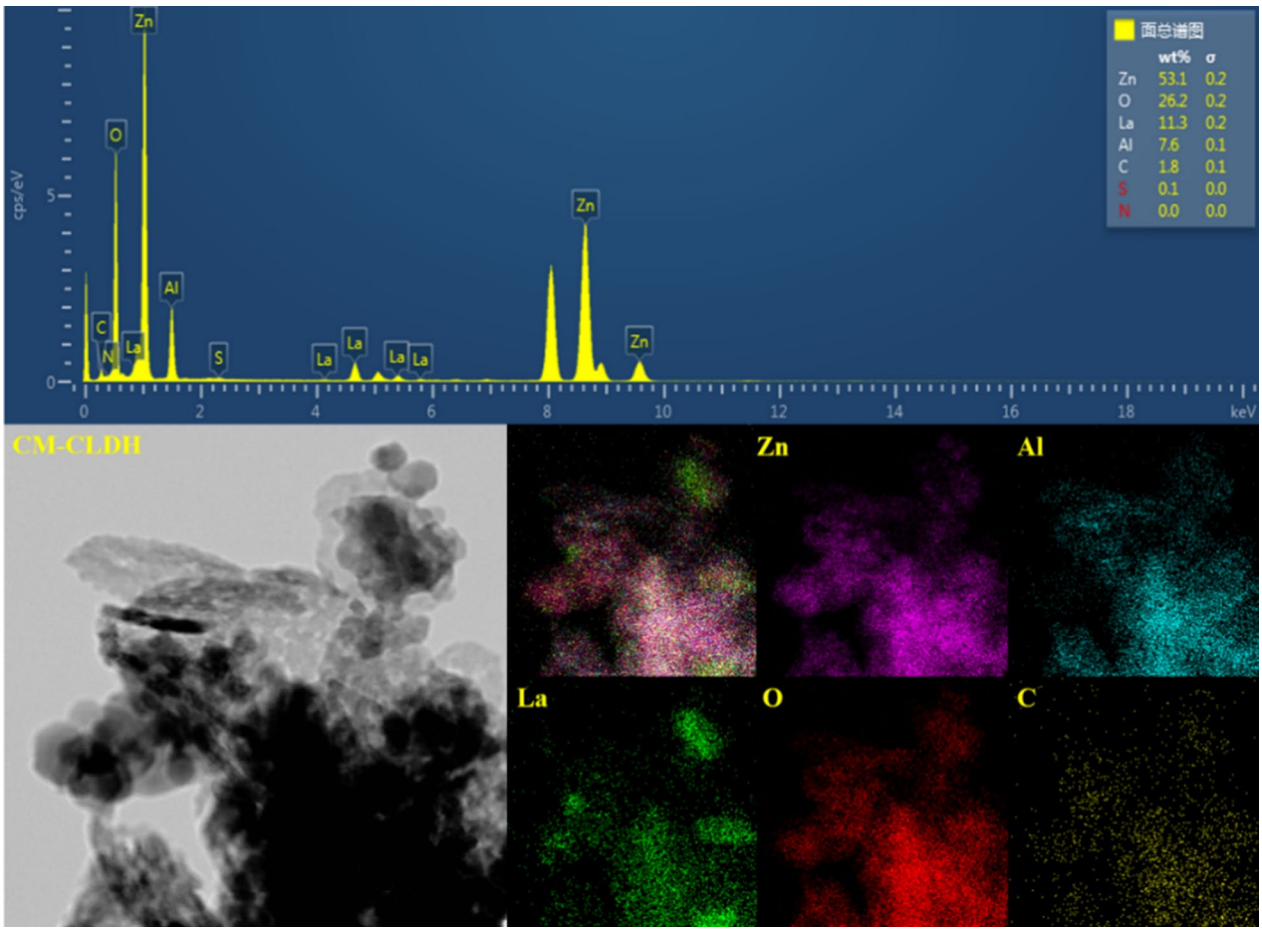

Fig. 3 Elemental mapping analysis of CM-CLDH

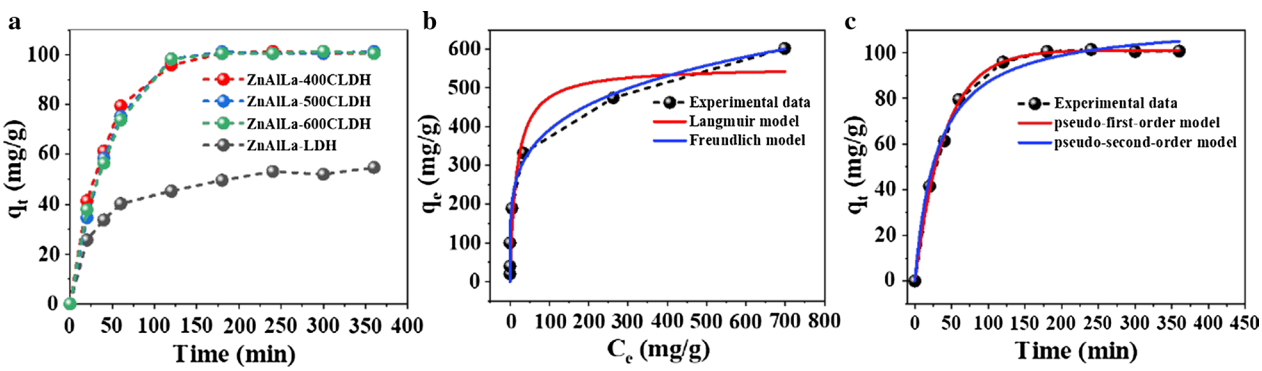

Fig. 4 Adsorption of amaranth (50 mg/L) by LDH/CLDHs as a function of time (**a**), adsorption kinetics of amaranth onto ZnAlLa-400CLDH (**b**), adsorption isotherm of amaranth onto ZnAlLa-400CLDH (**c**)

Adsorption kinetics and adsorption isotherms of amaranth on ZnAlLa-400CLDH were fitted by pseudo-first-order model and Freundlich isothem model, respectively. Detailed information was listed in Tables 1 and 2. Pseudo-first-order model was proposed by Lagergren; in this model, adsorbate-diffusion via a boundary occurred in advance of adsorption [41]. Adsorbent owing heterogeneous surface is the basic assumption of Freundlich

Table 1 Kinetic parameters for the adsorption of amaranth onto ZnAlLa-400CLDH

Sample	$q_{e,exp}$ (mg/g)	Pseudo-first-order model			Pseudo-second-order model		
		$q_{e,cal}$ (mg/g)	k_1 (min^{-1})	R^2	$q_{e,cal}$ (mg/g)	k_2 ($*10^{-4}$ g mg^{-1} min^{-1})	R^2
ZnAlLa-400CLDH	100	100.1	0.025	0.999	114.0	2.853	0.988

Table 2 Isotherm parameters of adsorption of amaranth onto ZnAlLa-400CLDH

Sample	Langmuir equation				Freundlich equation		
	q_{exp} (mg/g)	q_m (mg/g)	K_L (L/m4g)	R^2	n	K_F (L/g)	R^2
ZnAlLa-400CLDH	602.5	555.6	0.059	0.911	4.549	142.3	0.949

isotherm. In this empirical model, adsorption was a heterogenetic process in which interactions between adsorbates were taken into account [42]. Besides, the increase of uptake capacity would lead to exponential reduction in binding energy of surficial multilayers from adsorbed ions [43]. Hence, a large amount of amaranth molecules might be adsorbed on the surface of ZnAlLa-400CLDH stacks by stacks, which was in consonance with SEM images.

Photocatalysis experiments

After getting adsorption equilibrium of 50 mg/L amaranth, the composite material CLDH-AM was sent to tubular furnace for calcination, and temperature was set at 400, 500 and 600 °C, respectively. The resulting materials were noted as 400CM-CLDH, 500CM-CLDH and 600CM-CLDH, then utilized as photocatalysts in Ibuprofen degradation experiments, and the detailed procedures were recorded in 2.5. Figure 5 shows recorded data of photodegradation process, X axis representing time (min) and Y axis representing the ratio of sampled solution's concentration (C) and initial concentration (C_0). The consequence (Fig. 5a) elucidated that when amount of carbon source was equal, composites calcined at 500 °C had a higher photodegradation efficiency.

To evaluate the effect of carbon source amount on photocatalytic efficiency, in the following step, ZnAlLa-400CLDH was stirred in amaranth solution (concentration controlled at 10, 20, 50, 100, respectively) overnight for amaranth thoroughly adsorbed by ZnAlLa-400CLDH. Then, resulting composites were calcined at 500 °C under nitrogen flow. Samples were correspondingly noted as CM-CLDH10, CM-CLDH20, CM-CLDH50, and CM-CLDH100. As displayed in Fig. 5b, with the decrease of adsorbed amaranth, the resulting catalysts exhibited higher working efficiency. As pointed out in the previous publication, excessive carbon material might trigger light harvesting competition between carbon material and semiconductor. Also, instead of improving electron transportation, excessive carbon material could act as a center for photo-induced carriers' recombination [44].

When compared with pristine CLDHs calcined at 400, 500 and 600 °C, CM-CLDH10 still presented obvious advantages, and curves of C/C_0 dropped rapidly especially in the first 60 min (Fig. 5c). Pseudo-first-order equation derived from Langmuir–Hinshelwood model was used to evaluate kinetics of photocatalytic process [45], the formula could be expressed as follows:

$$\ln(C_0/C) = k_{app} * t \quad (5)$$

where k_{app} represents the apparent pseudo-first-order rate constant, C_0 and C are pollutant concentration at the start and the end of reaction. Higher k_{app} value normally indicated faster photodegradation process of a catalyst, k_{app} of CM-CLDH10, pure ZnAlLa-CLDHs and their pseudo-first-order kinetic plots are shown in Fig. 5d. Obviously, CM-CLDH10 displayed the highest photodegradation rate. In addition, in CM-CLDH10 system, it removed more than 90% Ibuprofen with the least time consumption, which could be regarded as the most effective catalysts in this work. Moreover, CM-CLDH10 was collected via suction filtration after photocatalysis, and recycled sample was used in IBF photodegradation experiments for another four times to evaluate its recyclability and stability. As depicted in Additional file 1: Fig. S3, after five runs, photodegradation efficiency of CM-CLDH10 decreased from 94.9% to 89.7%, indicating promising recyclability and stability of synthesized catalyst.

Photodegradation mechanisms

Effect of solution pH

Original pH of 5 mg/L Ibuprofen solution in this experiment was 5.90. Nitric acid and sodium hydroxide (0.5 mol/L) were injected by syringe to regulate pH of Ibuprofen at 3, 5, 7 and 9 (3.06, 4.96, 6.96 and 9.05 in

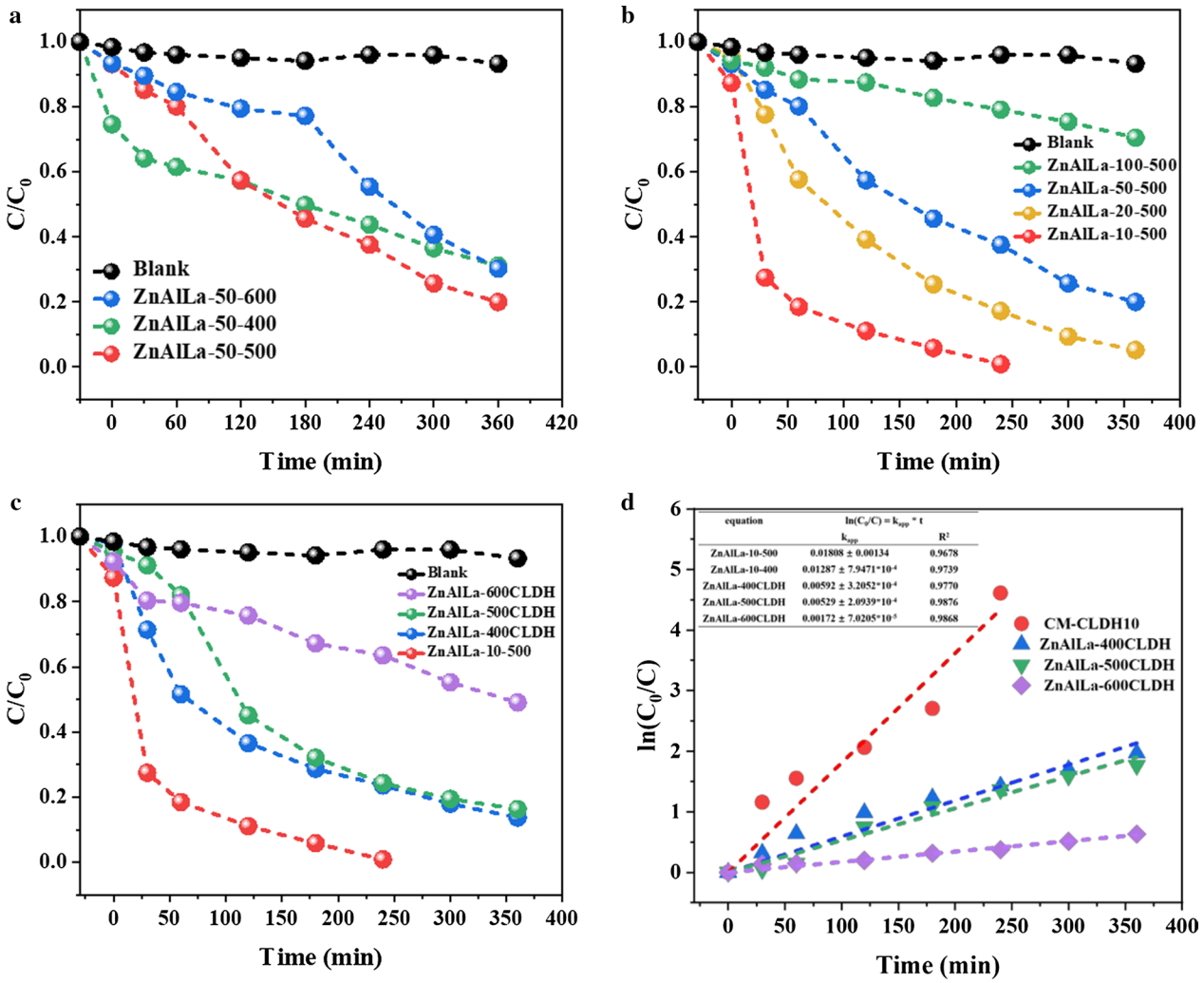

Fig. 5 Removal rate of Ibuprofen with CM-CLDH calcined under different teperature (**a**). Removal rate of Ibuprofen with CM-CLDH calcined under 500 °C (**b**). Comparison between CM-CLDH10 and CLDHs calcined at different temperature (**c**), psuedo-first-order plot under simulate sunlight with different catalysts (**d**)

effect). Photodegradation efficiencies over CM-CLDH10 under these four pH conditions are provided by Fig. 6a. With the decrease of pH values, CM-CLDH10 presented higher photodegradation efficiency; at pH = 3.06 more than 95% of target contaminant could be removed in 60 min, faster than that of other conditions. Interestingly, photodegradation rate gradually declined with the increase of pH value. Based on the former researches, acidic solutions could promote photodegradation through acceleration of ·OH manufacture [45]. Moreover, H^+ would react with $\cdot O_2^-$ to generate $HO\cdot_2$, both $\cdot O_2^-$ and $HO\cdot_2$ had clear advantage in ring cleavage of aromatic groups [46, 47]. According to scavenger experiment, effect of ·OH could be neglected, so attack of $\cdot O_2^-$ and $HO\cdot_2$ on Ibuprofen's aromatic ring might be indispensible during photodegradation. On the other hand, with the increase of pH, holes' oxidation ability would diminish due to cathodic displacement happened on valence band position [45]. And too many OH^- could also form hydrogen oxidation film during photocatalytic process, which hampered efficiency of catalysts [17].

Radical species detection

Radical species (RS) [mainly hydroxyl radical (·OH) and superoxide radical ($\cdot O_2^-$)] and singlet oxygen ($^1O_2$) play a vital role in photodegradation on organic contaminants. RS scavengers like tertiary butanol (BuOH), ethylenediaminetetraacetic acid disodium (EDTA-2Na), benzoquinone (BQ), $K_2Cr_2O_7$ and L-histidine were added into reaction system respectively to probe ·OH, holes

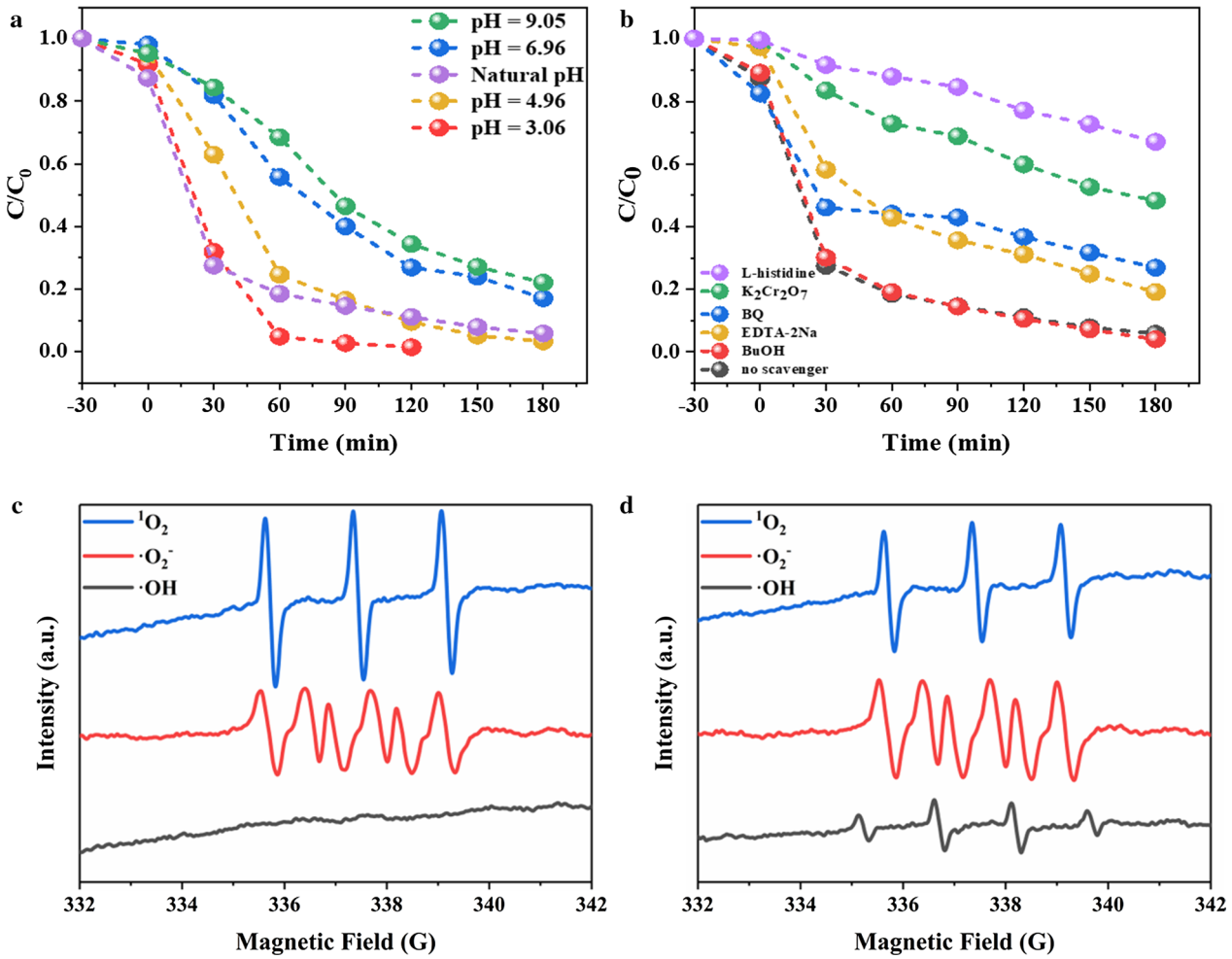

Fig. 6 Photodegradation efficiency over CM-CLDH10 under different pH conditions (**a**). Photodegradation efficiency over CM-CLDH10 with existence of different radical scavengers (**b**). ESR signals of $^1O_2$, $\cdot O_2$– and ·OH over ZnAlLa-500CLDH (**c**) and CM-CLDH10 (**d**)

(h^+), $\cdot O_2^-$, electrons (e^-) and $^1O_2$. As depicted in Fig. 6b, involvement of L-histidine, $K_2Cr_2O_7$ and BQ distinctly hampered efficiency and rate of photodegradation, which reflected singlet oxygen, electron and superoxide radical were dominant radicals during photocatalytic process [48–50]. On the contrary, addition of EDTA-2Na and BuOH showed limited inhibiting effect, revealing photo-induced holes and hydroxyl radicals' attack on Ibuprofen was relatively weak [50, 51].

Electronic spin resonance (ESR) test was also performed to investigate main radical species during photocatalytic process. As for hydroxyl radical and singlet oxygen, 5 mL water and 5 mg catalyst were added into quartz reaction dish, then severally injected 5 μL 5,5-Dimethyl-1-pyrroline N-oxide (DMPO) and 2,2,6,6-tetramethylpiperidine (TEMP) as spin-trapping agents. The resulting mixture was irradiated under an ultraviolet lamp for 5 min before being sampled in capillary tube for detection. Method for superoxide radical was similar, and the only difference was 5 mL water being substituted by 5 mL DMSO (dimethyl sulfoxide).

As shown in Fig. 6c, d, both ZnAlLa-500CLDH and CM-CLDH10 exhibited characteristic peaks of DMPO-$\cdot O_2^-$ and TEMP-$^1O_2$ with intensity ratio of 1:1:1:1:1:1 and 1:1:1. And relative intensity of DMPO-$\cdot O_2^-$ was higher in CM-CLDH10, suggesting involvement of carbonaceous material might lead to improvement of photodegradation. Moveover, after ultraviolet irradiation for 5 min, only CM-CLDH10 generated sufficient ·OH to be captured by DMPO; this evidence also reflected that combination with carbonaceous material could make CLDH present higher radical productivity, which might promote its photocatalytic performance.

Photoelectronic property

Photoluminescence (PL) signal would be generated at the time of photo-induced electrons and holes' recombination [52]; the higher intensity indicated lower separation efficiency of photo-generated carriers. With excitation wavelength set at 350 nm, PL signals of ZnAlLa-500CLDH and CM-CLDH10 were detected in the wavelength range of 365–600 nm (Fig. 7a). The consequence reflected that PL signal intensity of CM-CLDH10 was lower, manifesting better separation ability of photo-induced electrons and holes, which might be an important factor for better photocatalytic performance over CM-CLDH10. Photocurrent transient curves were obtained; the transient photocurrent responses of CM-CLDH10 were much higher than that of ZnAlLa-500CLDH, revealing carbonaceous material had a positive effect on separation of electrons and holes [50]. This conclusion was further proved by transient photocurrent response. As reflected in Fig. 7b, stronger intensity has been spotted on CM-CLDH10, which was triggered by higher separation efficiency of photo-induced h^+ and e^- [53].

Electrochemical impedance spectroscopy (EIS) curves were applied to assess electrochemical performances of synthesized materials. In this test, 1 mol L^{-1} sodium hydroxide carbon rod and saturated calomel electrode were utilized as electrolyte, counter electrode and reference electrode.

Figure 7c exhibits EIS plots of both catalysts, applied potential was 1.5 V (versus RHE) from 1000 kHz to 0.01 Hz in 1.0 mol L^{-1} sodium hydroxide electrolyte. Much larger semicircle's radius in Nyquist plot was connected with worse charge transfer resistance [54]. On the basis of PL, photocurrent and EIS test, photo-induced electrons and holes were generated mainly by CLDH's MO_6 octahedra which shared Metal–Oxygen bonds [55], and introduction of carbonaceous material could reduce recombination of photo-induced carriers. Nevertheless, its conductive activity was lower than pure metal or metal oxide, which might explain why photodegradation efficiency was falling down with the increasing amount of carbonaceous material on ZnAlLa-CLDH.

Energy band structure

According to UV–vis/DRS spectra, with increase of adsorbed amaranth amount, UV absorbance spectrum of resulting calcination product shifted to longer wavelength region, which suggested combination of carbonaceous material improved light adsorption [56]. Kubelka–Munk method-driven transformed reflectance spectra were attained to measure energy band (Eg) of ZnAlLa-500CLDH and CM-CLDH10 [57]; Eg values were 3.37 eV and 3.21 eV, and involvement of carbonaceous material narrowed band gap, which could improve photocatalytic activity. Mott–Schottky plots via implementing Mott–Schottky measurement was applied to estimate conduction band potential (E_{CB}) of prepared materials (saturated calomel electrode as reference electrode, 0.2 M Na_2SO_4 as electrolyte, pH = 7). As shown in Fig. 8c, d, E_{CB} values of n-type ZnAlLa-500CLDH and CM-CLDH10 were −0.71 V and −1.27 V (V vs NHE), after transformation from E (SCE) to E (NHE) [58]. As is known to all, $Eg = E_{VB} - E_{CB}$, calculated values of valence band potential (E_{VB}) were 2.66 V and 1.9 V.

According to aforementioned analysis, potential mechanism of photodegradation could be listed in the following equations and exhibited in Fig. 9.

$$CM - CLDH10 + h\nu \rightarrow e^- + h^+ \quad (6)$$

$$e^- + O_2 \rightarrow \cdot O_2^- \quad (7)$$

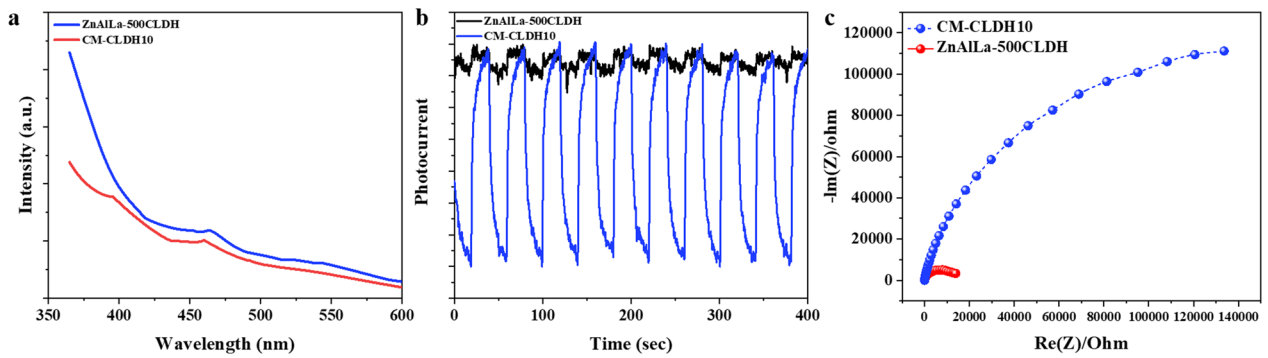

Fig. 7 Photoluminescence (PL) spectra (**a**), photocurrent plot (**b**) and EIS Nyquist plot (**c**) of ZnAlLa-500CLDH and CM-CLDH10

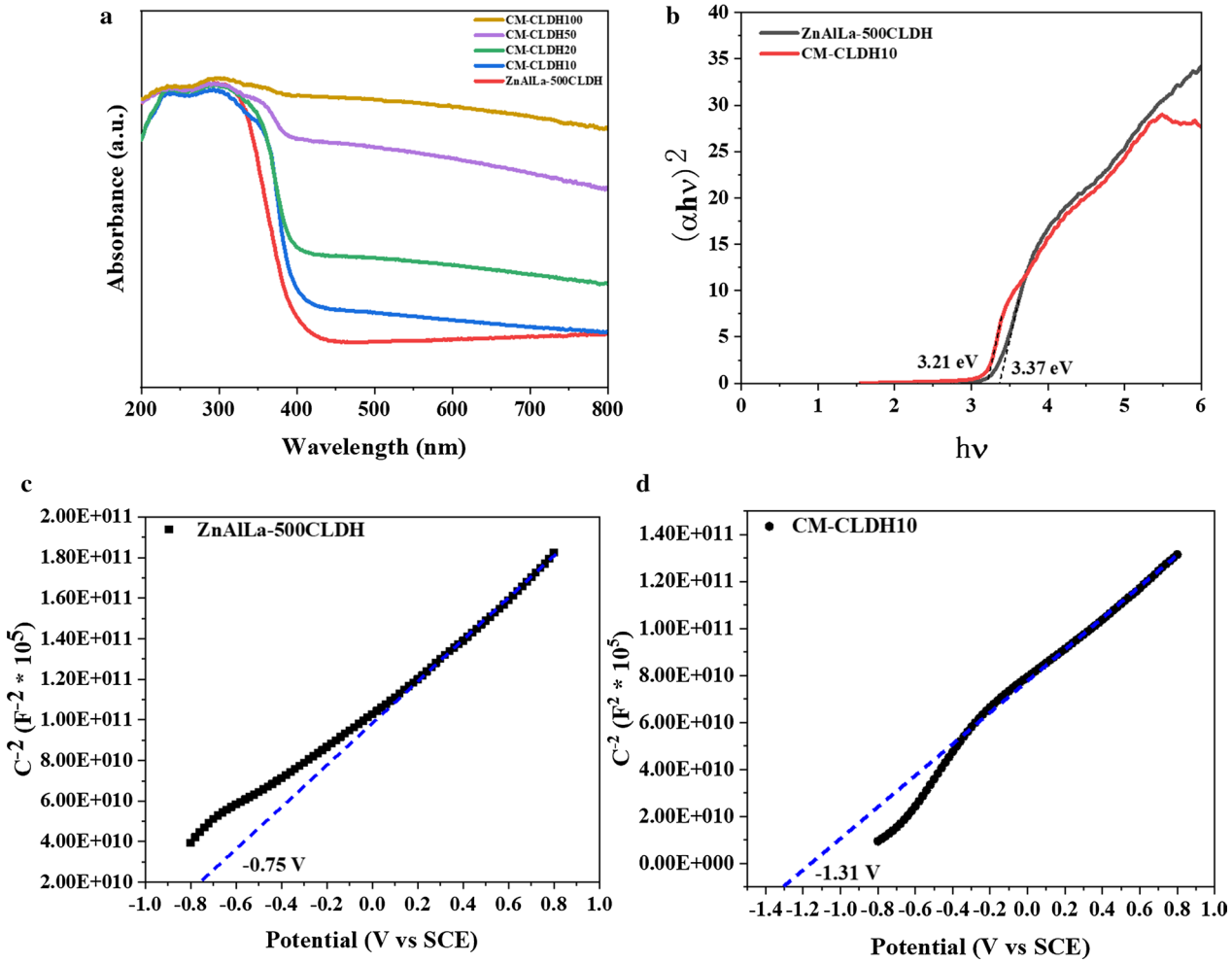

Fig. 8 UV–vis/DRS plot of synthesized samples (**a**), corresponding Kubelka–Munk transformed reflectance spectra of ZnAlLa-500CLDH and CM-CLDH10 (**b**), Mott-Schottky plots of ZnAlLa-500CLDH (**c**) and CM-CLDH10 (**d**)

$$H^+ + \cdot O_2^- \rightarrow HO\cdot_2 \quad (8)$$

$$\cdot O_2^- + h^+ \rightarrow {}^1O_2 \quad (9)$$

$$\text{Ibuprofen} + \cdot O_2^- \rightarrow \text{photocatalytic product} \quad (10)$$

$$\text{Ibuprofen} + HO\cdot_2 \rightarrow \text{photocatalytic product} \quad (11)$$

$$\text{Ibuprofen} + {}^1O_2 \rightarrow \text{photocatalytic product} \quad (12)$$

Conclusion

In summary, this study proved that calcined LDH can effectively remove azo dye through "memory effect"-driven adsorption. After calcination under nitrogen atmosphere, the resulting carbonaceous composite material exhibited higher photocatalytic activity, more than 90% of Ibuprofen could be removed under light irradiation (> 320 nm) in less than 180 min. Compered with pure CLDHs, CM-CLDH could hamper recombination of photo-induced carriers, supported by PL and photocurrent plots. And lower band gap (3.21 eV) enabled CM-CLDH to improve light adsorption. The composite catalyst could generate $\cdot O_2$;, $^1O_2$ to oxidize Ibuprofen, in low pH range, generation of $HO\cdot_2$ would accelerate collapse of aromatic nucleus. All these properties contributed to CM-CLDH's high efficiency in Iburofen removal experiments. This work has provided a strategy to reuse the spent adsorbent

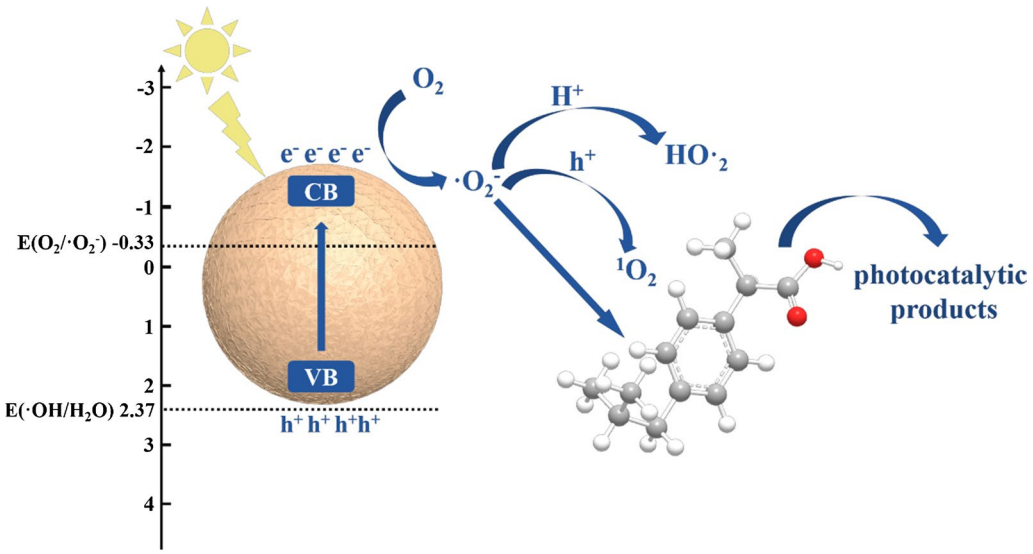

Fig. 9 Schematic diagram of Ibuprofen photodegradation process over CM-CLDH10

after treatment of organic pollutants for preparation of novel carbonaceous functional materials. It shows a potential to reduce second pollution of spent adsorbents in environment and to recycle adsorbent materials. The detailed mineralization efficiency and related biotoxicity of the pollutant during photodegradation process need to be investigated in a further study.

Supplementary information

Supplementary information accompanies this paper at https://doi.org/10.1186/s12302-020-00351-4.

Additional file 1: Fig. S1. XPS patterns of CM-CLDH and used CM-CLDH. **Fig. S2.** Thermogravimetry curves of ZnAlLa-LDH (a), amaranth (b) and CLDH-AM (c). **Fig. S3.** Photocatalytic efficiency of the catalyst for several runs.

Abbreviations

CLDH: Calcined layered double hydroxide; CM-CLDH: Carbonaceous material-CLDH; AM: Amaranth; IBF: Ibuprofen; XRD: X-ray diffractometry; FTIR: Fourier transform infrared spectroscopy; SEM: Scanning electron microscope; TEM: Transmission electron microscope; UPLC: Ultra-performance liquid chromotography; PL: Photoluminescence; EIS: Electrochemical impedance spectroscopy; RS: Radical species; DMPO: 5,5-Dimethyl-1-pyrroline N-oxide; TEMP: 2,2,6,6-tetramethylpiperidine; DMSO: Dimethyl sulfoxide; BuOH: Tertiary buthanol; BQ: Benzoquinone; EDTA-2Na: Ethylenediaminetetraacetic acid disodium.

Acknowledgements

Thanks to the funding support of Ministry of Science and Technology of China.

Authors' contributions

XS performed experiments, data analysis, and wrote the manuscript. ZZ gave the guidance to experiment design and made a detailed manuscript discussion and modification. TC and GD made contributions to some experiment designs. YQ and HZ gave guidance and support on instrumental analysis. DY gave substantial suggestions on experimental design. All authors read and approved the final manuscript.

Funding

This work was supported by National Science and Technology Major Project of China (Grant No. 2017ZX07201005).

Availability for data and materials

All data generated or analysed during this study are included in this published article [and its additional files].

Ethics approval and consent to participate

Not applicable.

Consent for publication

Not applicable.

Competing interests

The authors declare that they have no competing interests.

Author details

[1] Key Laboratory of Yangtze River Water Environment, Ministry of Education, Tongji University, Shanghai 200092, China. [2] State Key Laboratory of Pollution Control and Resource Reuse, Tongji University, Shanghai 200092, China. [3] Shanghai Institute of Pollution Control and Ecological Security, Shanghai 200092, China.

Received: 1 December 2019 Accepted: 27 April 2020
Published online: 11 May 2020

References

1. Zhang G, Ma Y (2013) Mechanistic and conformational studies on the interaction of food dye amaranth with human serum albumin by multispectroscopic methods. Food Chem 136(2):442–449
2. Barros WRP, Steter JR et al (2016) Catalytic activity of Fe3 — xCuxO4 ($0 \leq x \leq 0.25$) nanoparticles for the degradation of Amaranth food dye by heterogeneous electro-Fenton process. Appl Catal B 180:434–441
3. Abdellaoui K, Pavlovic I et al (2017) A comparative study of the amaranth azo dye adsorption/desorption from aqueous solutions by layered double hydroxides. Appl Clay Sci 143:142–150
4. Santos RMM, Tronto J et al (2017) Thermal decomposition and recovery properties of ZnAl–CO_3 layered double hydroxide for anionic dye adsorption: insight into the aggregative nucleation and growth mechanism of the LDH memory effect. J Mater Chem A 5(20):9998–10009

5. Zhang Y, He P et al (2019) Ti/PbO2-Sm2O3 composite based electrode for highly efficient electrocatalytic degradation of alizarin yellow R. J Colloid Interface Sci 533:750–761
6. Nath I, Chakraborty J et al (2018) Engineered synthesis of hierarchical porous organic polymers for visible light and natural sunlight induced rapid degradation of azo, thiazine and fluorescein based dyes in a unique mechanistic pathway. Appl Catal B 227:102–113
7. Shan R-r, Yan L-g et al (2014) Magnetic Fe3O4/MgAl-LDH composite for effective removal of three red dyes from aqueous solution. Chem Eng J 252:38–46
8. Lei C, Pi M et al (2017) Organic dye removal from aqueous solutions by hierarchical calcined Ni–Fe layered double hydroxide: isotherm, kinetic and mechanism studies. J Colloid Interface Sci 496:158–166
9. Lu H, Zhu Z et al (2015) Simultaneous removal of arsenate and antimonate in simulated and practical water samples by adsorption onto Zn/Fe layered double hydroxide. Chem Eng J 276:365–375
10. Cai J, Zhao X et al (2018) Enhanced fluoride removal by La-doped Li/Al layered double hydroxides. J Colloid Interface Sci 509:353–359
11. Lei C, Zhu X et al (2017) Superb adsorption capacity of hierarchical calcined Ni/Mg/Al layered double hydroxides for Congo red and Cr(VI) ions. J Hazard Mater 321:801–811
12. Zaghouane-Boudiaf H, Boutahala M et al (2012) Removal of methyl orange from aqueous solution by uncalcined and calcined MgNiAl layered double hydroxides (LDHs). Chem Eng J 187:142–149
13. Laipan M, Fu H et al (2017) Converting spent Cu/Fe layered double hydroxide into Cr(VI) reductant and porous carbon material. Sci Rep 7(1):7277
14. Laipan M, Zhu R et al (2015) From spent Mg/Al layered double hydroxide to porous carbon materials. J Hazard Mater 300:572–580
15. Daud M, Kamal MS et al (2016) Graphene/layered double hydroxides nanocomposites: a review of recent progress in synthesis and applications. Carbon 104:241–252
16. Liang J, Wei Y et al (2019) Constructing high-efficiency photocatalyst for degrading ciprofloxacin: three-dimensional visible light driven graphene based NiAlFe LDH. J Colloid Interface Sci 540:237–246
17. Ju L, Wu P et al (2017) Synthesis and characterization of Fullerene modified ZnAlTi-LDO in photo-degradation of Bisphenol A under simulated visible light irradiation. Environ Pollut 228:234–244
18. Zhu J, Zhu Z et al (2018) Calcined layered double hydroxides/reduced graphene oxide composites with improved photocatalytic degradation of paracetamol and efficient oxidation–adsorption of As(III). Appl Catal B 225:550–562
19. Ni J, Xue J et al (2017) Construction of magnetically separable NiAl LDH/Fe_3O_4-RGO nanocomposites with enhanced photocatalytic performance under visible light. Phys Chem Chem Phys 20(1):414
20. Mohamed F, Abukhadra MR et al (2018) Removal of safranin dye from water using polypyrrole nanofiber/Zn–Fe layered double hydroxide nanocomposite (Ppy NF/Zn–Fe LDH) of enhanced adsorption and photocatalytic properties. Sci Total Environ 640–641:352–363
21. Di G, Zhu Z et al (2017) Simultaneous removal of several pharmaceuticals and arsenic on Zn–Fe mixed metal oxides: combination of photocatalysis and adsorption. Chem Eng J 328:141–151
22. Shaban M, Abukhadra MR et al (2018) Recycling of glass in synthesis of MCM-48 mesoporous silica as catalyst support for Ni2O3 photocatalyst for Congo red dye removal. Clean Technol Environ Policy 20(1):13–28
23. Dong S, Xia L et al (2018) Controlled synthesis of flexible graphene aerogels macroscopic monolith as versatile agents for wastewater treatment. Appl Surf Sci 445:30–38
24. Tan L, Yu C et al (2019) Synergistic effect of adsorption and photocatalysis of 3D g-C3N4-agar hybrid aerogels. Appl Surf Sci 467–468:286–292
25. Vebber MC, Aguzzoli C et al (2019) Self-assembled thin films of PAA/PAH/TiO_2 for the photooxidation of ibuprofen. Part II: characterization, sensitization, kinetics and reutilization. Chem Eng J 361:1487–1496
26. Tzompantzi Carrera Y et al (2013) ZnO–Al2O3–La2O3 layered double hydroxides as catalysts precursors for the esterification of oleic acid fatty grass at low temperature. Catal Today 212:164–168
27. Busetto C, Del Piero G et al (1984) Catalysts for low-temperature methanol synthesis. Preparation of Cu–Zn–Al mixed oxides via hydrotalcite-like precursors. J Catal 85(1):260–266
28. Zhu J, Zhu Z et al (2016) Enhanced photocatalytic activity of Ce-doped Zn–Al multi-metal oxide composites derived from layered double hydroxide precursors. J Colloid Interface Sci 481:144–157
29. Zhao Q, Tian S et al (2015) Novel HCN sorbents based on layered double hydroxides: sorption mechanism and performance. J Hazard Mater 285:250–258
30. Lupa L, Cocheci L et al (2018) Phenol adsorption using Aliquat 336 functionalized Zn-Al layered double hydroxide. Sep Purif Technol 196:82–95
31. Guo Y, Zhu Z et al (2013) Enhanced adsorption of acid brown 14 dye on calcined Mg/Fe layered double hydroxide with memory effect. Chem Eng J 219:69–77
32. José dos Reis M, Silvério F et al (2004) Effects of pH, temperature, and ionic strength on adsorption of sodium dodecylbenzenesulfonate into Mg–Al–CO_3 layered double hydroxides. J Phys Chem Solids 65(2):487–492
33. Zhao Y, Chen G et al (2015) Defect-rich ultrathin ZnAl-layered double hydroxide nanosheets for efficient photoreduction of CO_2 to CO with water. Adv Mater 27(47):7824–7831
34. Seo Y, Choi T-Y et al (2015) Enhancement of stability of aqueous suspension of alumina nanoparticles by femtosecond laser irradiation. J Appl Phys 118(11):114906
35. Li H, Xin C et al (2015) Direct carbonylation of glycerol with CO_2 to glycerol carbonate over Zn/Al/La/X (X=F, Cl, Br) catalysts: the influence of the interlayer anion. J Mol Catal A: Chem 402:71–78
36. Huang Z, Wang T et al (2019) Coagulation treatment of swine wastewater by the method of in situ forming layered double hydroxides and sludge recycling for preparation of biochar composite catalyst. Chem Eng J 369:784–792
37. Gao Z, Sasaki K et al (2018) Structural memory effect of Mg-Al and Zn-Al layered double hydroxides in the presence of different natural humic acids: process and mechanism. Langmuir 34(19):5386–5395
38. Wang R-X, Wen T et al (2014) Highly efficient removal of humic acid from aqueous solutions by Mg/Al layered double hydroxides—Fe_3O_4 nanocomposites. RSC Advances 4(42):21802–21809
39. Gasser MS, Mohsen HT et al (2008) Humic acid adsorption onto Mg/Fe layered double hydroxide. Colloids Surf A 331(3):195–201
40. Kutlu B, Leuteritz A et al (2014) Stabilization of polypropylene using dye modified layered double hydroxides. Polym Degrad Stab 102:9–14
41. Ahmed IM, Gasser MS (2012) Adsorption study of anionic reactive dye from aqueous solution to Mg–Fe–CO_3 layered double hydroxide (LDH). Appl Surf Sci 259:650–656
42. Wang X, Jiang C et al (2018) Carbon composite lignin-based adsorbents for the adsorption of dyes. Chemosphere 206:587–596
43. Bagherifam S, Komarneni S et al (2014) Highly selective removal of nitrate and perchlorate by organoclay. Appl Clay Sci 95:126–132
44. Dong S, Ding X et al (2017) Self-assembled hollow sphere shaped Bi_2WO_6/RGO composites for efficient sunlight-driven photocatalytic degradation of organic pollutants. Chem Eng J 316:778–789
45. Wang X, Wu P et al (2014) Solar photocatalytic degradation of methylene blue by mixed metal oxide catalysts derived from ZnAlTi layered double hydroxides. Appl Clay Sci 95:95–103
46. Ng J, Wang X et al (2011) One-pot hydrothermal synthesis of a hierarchical nanofungus-like anatase TiO2 thin film for photocatalytic oxidation of bisphenol A. Appl Catal B 110:260–272
47. Zhang L-S, Wong K-H et al (2010) Effective photocatalytic disinfection of *E. coli* K-12 using AgBr—Ag—Bi2WO6 nanojunction system irradiated by visible light: the role of diffusing hydroxyl radicals. Environ Sci Technol 44(4):1392–1398
48. Yun E-T, Lee JH et al (2018) Identifying the nonradical mechanism in the peroxymonosulfate activation process: singlet oxygenation versus mediated electron transfer. Environ Sci Technol 52(12):7032–7042
49. Xie X, Zhang N et al (2018) Ti3C2Tx MXene as a Janus cocatalyst for concurrent promoted photoactivity and inhibited photocorrosion. Appl Catal B Environ 237:43–49
50. Jo W-K, Kim Y-G et al (2018) Hierarchical flower-like NiAl-layered double hydroxide microspheres encapsulated with black Cu-doped TiO_2 nanoparticles: highly efficient visible-light-driven composite photocatalysts for environmental remediation. J Hazard Mater 357:19–29
51. Najafian H, Manteghi F et al (2019) Fabrication of nanocomposite photocatalyst $CuBi_2O_4$/Bi_3ClO_4 for removal of acid brown 14 as water pollutant under visible light irradiation. J Hazard Mater 361:210–220

52. Liu X, Ma C et al (2013) Hydrothermal synthesis of CdSe quantum dots and their photocatalytic activity on degradation of cefalexin. Ind Eng Chem Res 52(43):15015–15023
53. Zang S, Zhang G et al (2019) Enhancement of photocatalytic H2 evolution on pyrene-based polymer promoted by MoS2 and visible light. Appl Catal B 251:102–111
54. Chen F, Yang Q et al (2017) Hierarchical assembly of graphene-bridged Ag3PO4/Ag/BiVO4 (040) Z-scheme photocatalyst: an efficient, sustainable and heterogeneous catalyst with enhanced visible-light photoactivity towards tetracycline degradation under visible light irradiation. Appl Catal B 200:330–342
55. Chen Y, Rui K et al (2019) Recent progress on nickel-based oxide/(oxy) hydroxide electrocatalysts for the oxygen evolution reaction. Chem A Eur J 25(3):703–713
56. Cho S, Lee K-H (2011) Formation of zinc aluminum mixed metal oxide nanostructures. J Alloy Compd 509(35):8770–8778
57. Ng J, Xu S et al (2010) Hybridized nanowires and cubes: a novel architecture of a heterojunctioned TiO_2/$SrTiO_3$ thin film for efficient water splitting. Adv Func Mater 20(24):4287–4294
58. Zheng J, Lei Z (2018) Incorporation of CoO nanoparticles in 3D marigold flower-like hierarchical architecture $MnCo_2O_4$ for highly boosting solar light photo-oxidation and reduction ability. Appl Catal B 237:1–8

Publisher's Note